

Mixed-Valence Ce-BPyDC Metal–Organic Framework with Dual Enzyme-like Activities for Colorimetric Biosensing

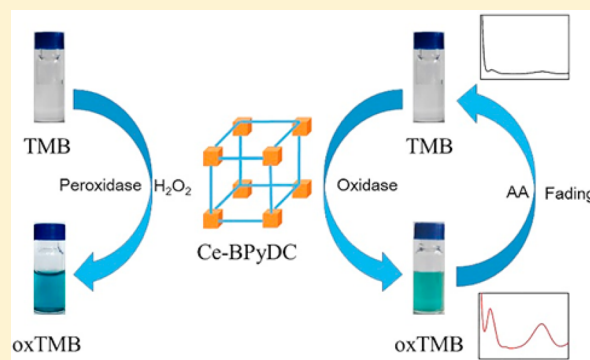
Linpin Luo,[†] Lunjie Huang,[†] Xinnan Liu,[†] Wentao Zhang,[†] Xiaolin Yao,[†] Leina Dou,[†] Xu Zhang,[†] Ying Nian,[‡] Jing Sun,[‡] and Jianlong Wang^{*,†}

[†]College of Food Science and Engineering, Northwest A&F University, Yangling 712100, Shaanxi, China

[‡]Qinghai Provincial Key Laboratory of Qinghai-Tibet Plateau Biological Resources, Northwest Institute of Plateau Biology, Chinese Academy of Sciences Qinghai, Xining 810008, China

Supporting Information

ABSTRACT: Enzyme-like metal–organic frameworks (MOFs) are currently one type of starring material in the fields of artificial enzymes and analytical sensing. However, there has been little progress in making use of the MOF structures based on the catalytically active metal center with multiple valences. Herein, we report a mixed-valence Ce-MOF (Ce-BPyDC) that can exhibit both oxidase-like and peroxidase-like activities. Ce-BPyDC was synthesized by a facile hydrothermal method, which preserves the rare coexistence of Ce(III) and Ce(IV) in the MOF structure. The enzymatic studies demonstrated the enzyme-like activities of Ce-BPyDC follow the Michaelis–Menten kinetics and are strongly dependent on temperature, pH, and reaction time. Ce-BPyDC was also revealed to exert high catalytic activity that could transcend horseradish peroxidase and other MOF nanozymes, due to the redox-active Ce(III)/Ce(IV) cycles inside. Furthermore, the simple synthesis, high nanozyme activity, and great stability of Ce-BPyDC motivated us to establish a colorimetric biosensing platform using 3,3',5,5'-tetramethylbenzidine as a color reagent. Adopting this strategy, we established a visual, sensitive, and selective colorimetric method for ascorbic acid (AA) detection, for which the linear interval and limit of detection were 1–20 and 0.28 μM , respectively. The successful AA detection in real juice samples implies the promising use of such mixed-valence MOF nanozymes in food and biomedical samples.



INTRODUCTION

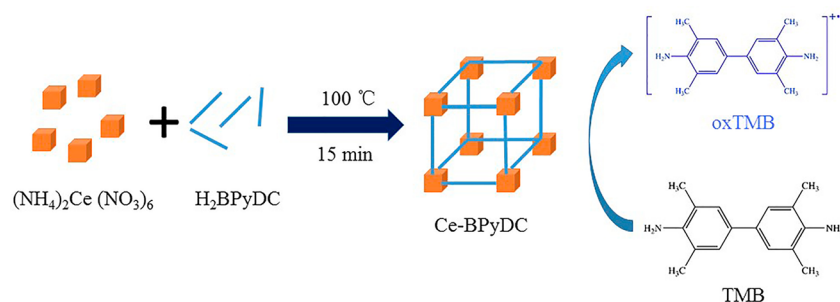
Natural enzymes, such as the biomolecule catalysts, can specifically catalyze chemical reactions under mild conditions.¹ These biocatalysts, such as horseradish peroxidase (HRP), glucose oxidase, acetylcholinesterase (AChE), and alkaline phosphatase (ALP), were widely used in analytical applications, including in the enzyme-linked immunosorbent assay, as colorimetric and electrochemical sensors, and in the lateral flow immunoassay in previous studies. However, natural enzymes have disadvantages, such as vulnerability to a harsh environment, low operational stability, high costs, etc.² Therefore, the artificial enzyme mimics, especially nanozymes, which could make up for the shortcomings of natural enzymes, have received widespread attention.² Until now, a number of nanomaterials, such as noble metal nanoparticles (NPs),³ metal oxides,^{4–6} oxy-hydroxide,^{7,8} bimetal oxides,⁹ carbon materials,¹⁰ and transition metal disulfides,¹¹ were found to exhibit intrinsic enzyme-like activities. In particular, recent works have proved that nanozymes with a high surface-to-volume ratio always possess high catalytic activity, which is attributed to the abundance of catalytic sites and affinity sites toward colorimetric substrates.^{10–14} Hence, screening of

nanomaterials with a high surface-to-volume ratio is the key to optimizing the activities of nanozymes.

Metal–organic frameworks (MOFs) are a type of organic–inorganic coordination compound formed by the assembly of organic ligands and metal ions or clusters,¹⁵ which have shown great potential in biosensing and imaging, adsorption and separation, heterogeneous catalysis, and cancer therapy.^{16–19} Owing to their large surface area, abundant active sites, and designable structures, MOF materials are well suited to being candidates for nanozyme exploitation. In previous studies, many kinds of MOFs have been explored for enzyme-like catalysis,²⁰ such as the peroxidase-like Fe-MOFs (MIL-53, MIL-68, MIL-100, MIL-88A, MIL-88-NH₂, and MIL-101),²¹ Cu-MOFs (Cu-BTC, Cu-hemin MOFs, HKUST-1, and Hemin@HKUST-1),²² Zr-MOFs (UiO-66-NH₂ and Pt NP@UiO-66-NH₂),²³ Zn-MOFs (BHb@ZIF-8, GOx@mZIF-8, and GOx/hemin@ZIF-8),²⁴ Co-MOF (CoNPs/MC and Co/2Fe-MOF),²⁵ Ni-MOF nanosheets,²⁶ Al-MOF [Hemin@MIL-101(Al)NH₂],²⁷ and oxidase-like Co/2Fe-MOF.²⁵ As such, various high-performance sensing platforms have been

Received: March 6, 2019

Scheme 1. Illustration of Colorimetric Detection of AA by Using Ce-BPyDC as a Catalyst



established on such MOF nanozymes for the detection of ions, small biomolecules, pesticides, DNA, and bacteria.²⁸ To summarize, these MOF nanozymes share the following features. (1) The active catalytic centers are highly dependent on the redox-active metal elements. (2) MOFs with more than one metal element or a metal element of mixed valences tend to process higher catalytic activities. (3) The chemical stability of MOFs is a key parameter for reproducible catalytic performance. However, the current MOF nanozymes process either weak catalytic activities, limited dispersion stability, or low environmental tolerance, which hinders their scalable uses at present. In this regard, finding an excellent MOF enzyme that mimics the positive features mentioned above would be beneficial.

Cerium, as an important rare earth element,²⁹ has been widely utilized in the field of catalysis. More and more cerium-based nanomaterials have been developed as catalysts due to their unique advantages.³⁰ For instance, cerium dioxide (CeO_2) is one of the most popular industrial catalysts or catalyst supports and plays a critically important role in the development of three-way catalysts.³¹ Moreover, the superiority of CeO_2 , which originated from a redox-active Ce element, also strongly promoted the development of mimetic enzymes.^{5,32} In contrast, the MOF structures with Ce centers were rarely involved in nanozyme-related research projects,^{33,34} which could be a point of penetration for improving the applicability of MOF nanozymes.

Herein, we synthesize a new type of MOF (Ce-BPyDC) with a mixed-valence Ce element as the metal center that possesses dual enzyme activities (peroxidase and oxidase). As shown in Scheme 1, Ce-BPyDC could catalyze the chromogenic substrates, such as 3,3',5,5'-tetramethylbenzidine (TMB), *o*-phenylenediamine (OPD), and 2,2'-azinobis(3-ethylbenzthiazoline-6-sulfonic acid) (ABTS), to produce colorimetric oxidation products in the presence or absence of H_2O_2 . The catalysis of such a MOF nanozyme strongly depends on the reaction temperature and solution pH and follows Michaelis–Menten behavior. Moreover, the catalytic mechanism studies demonstrated that the nanozyme properties of Ce-BPyDC were a consequence of the Ce(III)/Ce(IV) redox cycles inside the Ce-BPyDC nanostructure. Finally, we established a colorimetric method for highly sensitive detection of ascorbic acid (AA) based on the oxidase activity of Ce-BPyDC, which was further applied in the real fruit juice samples.

RESULTS AND DISCUSSION

Characterization of Ce-BPyDC. Scanning electron microscopy (SEM) and transmission electron microscopy (TEM) images were collected to investigate the surface

morphology and size of the as-prepared Ce-BPyDC. As shown in Figure 1a and Figure S1, most of the obtained Ce-

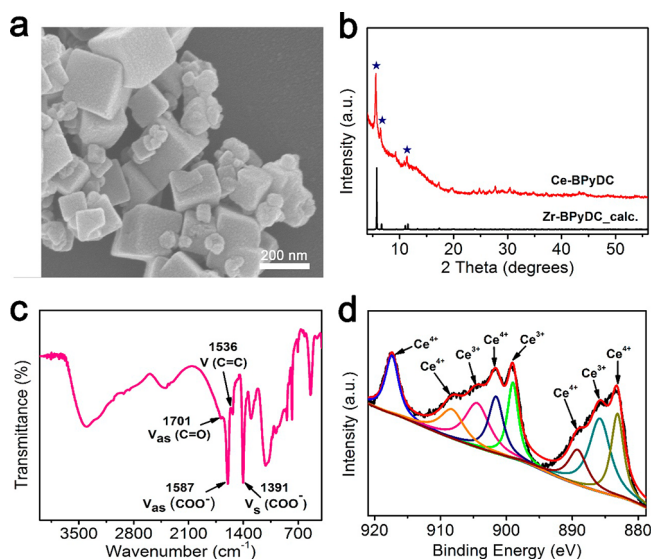


Figure 1. Structural characterizations of Ce-BPyDC: (a) SEM image, (b) XRD pattern, (c) IR spectral analysis, and (d) XPS spectra for the Ce 3d region of as-prepared Ce-BPyDC.

BPyDC particles exhibit a cube-like structure with a size of 200–250 nm, while some other particles are smaller (~100 nm). The crystalline structure of Ce-BPyDC was analyzed by the powder X-ray diffraction (XRD) technique (Figure 1b). The result showed that the as-obtained Ce-BPyDC exhibited the same crystalline structure that can be found in the literature.³⁵ The infrared (IR) spectrum of as-prepared Ce-BPyDC contains high-intensity peaks at around 1701, 1587, 1536, and 1391 cm^{-1} (Figure 1c), which are associated with asymmetric stretching vibrations for the carbonyl group ($\text{C}=\text{O}$), asymmetric stretching vibrations for the carbonyl group (COO^-) of the linker H_2BPyDC , aromatic rings ($\text{C}=\text{C}$), and stretching vibrations for the carbonyl group (COO^-) of the linker, respectively.³⁵ Finally, the high-resolution X-ray photoelectron spectroscopy (XPS) spectra of Ce 3d, C 1s, and O 1s were obtained. As shown in Figure S2, the C 1s peaks centered at 284.7 and 288.6 eV are ascribed to C–C and $\text{C}=\text{O}$, respectively, while the O 1s peaks centered at 529.6, 531.4, and 533.0 eV are attributed to lattice oxygen (Ce–O), $\text{C}=\text{O}/\text{OH}$, and C–O, respectively.³⁶ More importantly, as shown in Figure 1d, the peaks at 917.4, 905.5, 901.6, 889.3, and 883.1 eV are related to the Ce(IV) state while the peaks at 904.7, 899.0, and 885.8 eV are related to the Ce(III) state. In

addition, the ratio of peak areas of Ce(III) and Ce(IV) states obtained from the Ce 3d spectrum is $\sim 1:1.2$. The thermogravimetric curves were obtained to evaluate the thermal stability of Ce-BPyDC. As shown in Figure S3, Ce-BPyDC kept losing H₂O molecules when the heating temperature was below 320 °C, and the linker molecules of Ce-BPyDC started to degrade over 320 °C, which demonstrated that Ce-BPyDC exhibits excellent thermal stability below 320 °C. The specific BET surface area and pore size calculated from the N₂ adsorption–desorption isotherm (Figure S4) are 1950 m² g⁻¹ and 0.82 cm³ g⁻¹, respectively, in good agreement with the parameters in ref 35. This result illustrates that the Ce-BPyDC particle has a large surface area and a high porosity. These results proved the successful preparation of Ce-BPyDC with Ce(III)/Ce(IV) mixed valences.

Enzyme-like Activities of Ce-BPyDC. The oxidase-like activity of Ce-BPyDC was tested by measuring the catalytic reaction of the TMB substrate without the participation of H₂O₂. As shown in Figure 2a, the Ce-BPyDC/TMB system

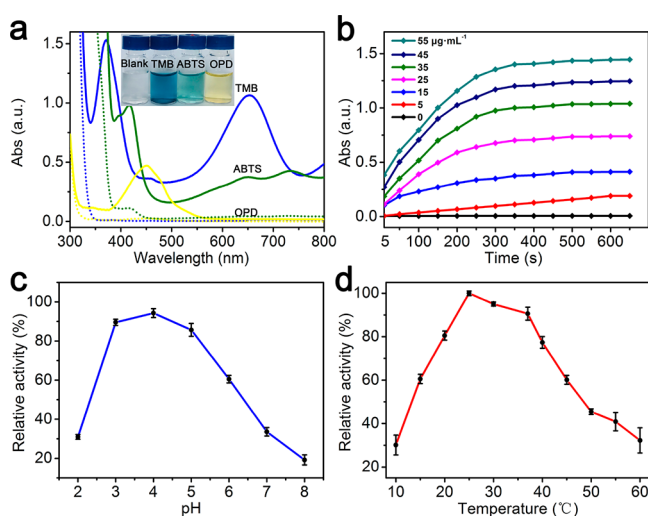


Figure 2. Oxidase-like catalytic properties of Ce-BPyDC. (a) Ultraviolet–visible absorption spectra from recording the oxidation of 1 mM ABTS (green line), TMB (blue line), and OPD (yellow line) catalyzed by Ce-BPyDC (25 μg mL⁻¹). The corresponding dashed line indicates the incubation of Ce-BPyDC with ABTS, TMB, or OPD only. Reaction time $t = 10$ min. (b) Time- and catalyst concentration-dependent absorbance at 652 nm measured from the reaction solutions containing 1 mM TMB and Ce-BPyDC at different concentrations in 0.1 M acetate buffer (pH 4.0) at room temperature. The oxidase-like catalytic activity of Ce-BPyDC vs (c) pH and (d) temperature. The maximum activity in each graph was set as 100%.

changed from colorless to blue and generated a high absorbance at 652 nm. In contrast, TMB only did not show a distinct difference in the color change or the absorption peak at 652 nm. These results indicated that Ce-BPyDC could catalyze the TMB. Meanwhile, several different chromogenic substrates like 2,2'-azino-bis(3-ethylbenzthiazoline-6-sulfonic acid) (ABTS) and *o*-phenylenediamine (OPD) were also tested. The results depicted in Figure 2a show that Ce-BPyDC also could catalyze the oxidation reaction of ABTS or OPD to give a green or yellow color and exhibit the corresponding absorption peaks at 415 and 447 nm, respectively.³⁷ This evidence proved that Ce-BPyDC exhibited intrinsic oxidase-mimicking activity. Furthermore, we investigated the perox-

idase-like activity of this material. Figure S5a shows the colors of the Ce-BPyDC/TMB/H₂O₂, Ce-BPyDC/ABTS/H₂O₂, and Ce-BPyDC/OPD/H₂O₂ solutions are blue, green, and yellow, respectively, with the corresponding absorption peaks located at 652, 415, and 447 nm, respectively, while the rest of the systems did not show color or absorbance changes in comparison with the experimental group. Therefore, Ce-BPyDCs can be developed as oxidase-like and peroxidase-like mimics.

To further optimize the enzyme activities of Ce-BPyDC, we explored the effects of reaction time, catalyst concentration, pH, and temperature on the enzymatic activity of Ce-BPyDC. Figure 2b and Figure S5b show the absorbance was time-dependent and changed with the concentration of Ce-BPyDC at 652 nm. The increasing concentration of Ce-BPyDC could enhance the reaction rates. Meanwhile, the absorbance increased with time and then remained constant after 10 min. Figures S6 and S7 show the relationship between activities and the concentrations of Ce-BPyDC, indicating that the enzymatic activity could be dramatically improved with an increase in the concentration of Ce-BPyDC. Similar to other nanomaterial-based enzyme mimics, the enzymatic activity of Ce-BPyDC relied greatly on pH and temperature. As shown in Figure 2c and Figure S5c, the high activities of Ce-BPyDC could be maintained over a pH range of 3.0–6.0 (oxidase-like) or 3.0–5.0 (peroxidase-like), in which a pH value of 4 was chosen for the catalytic reactions. The oxidase-like activity showed a slow increase as the reaction temperature increased, and the activity showed a downward trend when the temperature was above 40 °C (Figure 2d). The peroxidase-like reaction system (Figure S5d) showed an activity–temperature relationship similar to that of the oxidase reaction system. As such, the following studies were performed at 25 °C. The optimal reaction time was 10 min according to the time-dependent absorbance curve. In conclusion, the dual activities of Ce-BPyDC strongly depend on the catalyst concentration, pH, and solution temperature.

Stability and Reusability of Ce-BPyDC. The stability of Ce-BPyDC was evaluated in our research. To investigate the water dispersion of Ce-BPyDC, a certain amount of material was dispersed in water and stored for 7 days at room temperature. As shown in Figure S8, Ce-BPyDC exhibited no obvious aggregation in solution, proving its excellent aqueous dispersity. The catalytic stability of Ce-BPyDC was examined by measuring the enzymatic activity changes over time. As shown, the Ce-BPyDC could remain over 90% of the oxidase-like activity (Figure S9a) and peroxidase-like activity (Figure S9b) after being stored for 20 days. In addition, the physicochemical stability was also examined by TEM analysis, XRD patterns, and Fourier transform infrared (FT-IR) measurements before and after the catalytic reaction. The results (Figure S10) show that there are no significant changes in TEM images, XRD patterns, or FT-IR spectra of Ce-BPyDC before and after catalysis, which indicated that Ce-BPyDC can remain stable during the catalytic reaction.

We also evaluated the enzyme activities of five different batches of Ce-BPyDC (Figure S11). As shown, Ce-BPyDCs exhibited small differences (<10%) in their enzyme activities between batches; thus, we can conclude that Ce-BPyDC possesses excellent batch-to-batch reproducibility. After that, to evaluate the cycle performance of Ce-BPyDC as a catalyst, the enzymatic activities were examined during repetitive cycles (Figure S12). The results show that >85% of dual nanzyme

activities were maintained even after eight repetitive cycles, indicating the good reusability of Ce-BPyDC and its detection platform. The excellent stability and reusability of Ce-BPyDC are greatly significant for the establishment of a colorimetric probe.

Catalytic Mechanism of Ce-BPyDC. The possible catalytic mechanisms of Ce-BPyDC were also investigated. The catalytic activities of Ce-BPyDC after centrifugation were measured, and the obtained values were compared with those of the original solutions. The results show no obvious difference in catalytic activities (Figure S13), which manifested that the dissolved ions in solution made no contribution to the catalytic reaction of Ce-BPyDC. As previously reported, the possible mechanism of oxidase-like activity for Ce-based materials might originate from the Ce(III)/Ce(IV) system that the Ce-based materials possess.^{33,36} In our work, as shown in Figure S14, the possible mechanism behind the oxidase-like activity of Ce-BPyDC might originate from the Ce(III)/Ce(IV) couple that the cerium materials retain, in which these species can balance between the two Ce(III)/Ce(IV) valences in redox-active reactions. The Ce(IV) ions were reduced to Ce(III) ions during the TMB oxidation reaction. Then, the generated Ce(III) ions “spontaneously” recycle back to the Ce(IV) ions. The possible mechanisms of peroxidase-like activity were also explored. The hydroxyl radical ($\bullet\text{OH}$), a common intermediate during the peroxidase-like catalytic reaction, is usually deemed to be the key to peroxidase-like catalytic activity. Terephthalic acid (TA) could combine with $\bullet\text{OH}$ and form a fluorescent product called 2-hydroxyterephthalic acid (TAOH).³⁸ Therefore, the $\bullet\text{OH}$ possibly generated during the peroxidase-like reaction was monitored by fluorescence experiments. Figure S15 presents the fluorescence image of the mixed solution of Ce-BPyDC, TA, and H_2O_2 after incubation for 12 h at 37 °C. The Ce-BPyDC, TA, and H_2O_2 mixed solution exhibited a high fluorescence intensity at 425 nm compared with those of control experiments. *tert*-Butyl alcohol can capture $\bullet\text{OH}$ radicals and scavenge them. Therefore, colorimetric tests were also carried out to further prove the generation of $\bullet\text{OH}$ during the reaction.³⁹ As shown in Figure S16, *tert*-butyl alcohol could attenuate the absorption intensity at 652 nm within a concentration range of 0–400 mg mL^{-1} . These results indicated the generation of $\bullet\text{OH}$ radicals in the peroxidase system.

The steady-state kinetic testing was performed on the Ce-BPyDC/TMB system to gain more details about the oxidase catalytic properties. A typical Michaelis–Menten curve was obtained by plotting the corresponding initial reaction velocities versus the substrate concentration (Figure 3a). By taking the double reciprocal of the data in Figure 3a, we obtained the Lineweaver–Burk plot (Figure 3b), in which the slope and intercept of the curve represent Michaelis–Menten constants (K_m) and maximum initial reaction rates (V_{max}), respectively. K_m was considered a parameter for evaluating the affinity between enzymes and substrates. The enzymes with a strong affinity for a substrate always have a low K_m value. As shown in Table S1, the K_m and V_{max} of Ce-BPyDC with TMB as a substrate were 0.12 mM and 20.6×10^{-8} M/s, respectively. Ce-BPyDC exhibits a K_m value that is lower than that of other oxidase-like nanozymes, indicating that the smaller amount of TMB was needed to achieve maximum catalytic activity for Ce-BPyDC. The low K_m value, the Ce(III)/Ce(IV) balance, accompanied by the adsorption nature of MOF structure, may contribute to a high binding

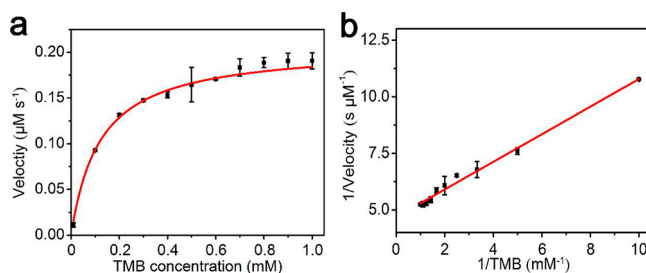


Figure 3. Steady-state kinetic analysis of Ce-BPyDC as an oxidase mimetic. (a) Oxidase-like activity system with different concentrations of H_2O_2 . (b) Double-reciprocal plots of $25 \mu\text{g mL}^{-1}$ Ce-BPyDC in acetate buffer (pH 4.0) at room temperature.

affinity of Ce-BPyDC for a catalytic substrate. In addition, Ce-BPyDC possessed a V_{max} value equal to or even higher than those of other reported oxidase mimics. To gain more information about the Ce-BPyDC peroxidase-like property, the steady-state kinetic parameters for Ce-BPyDC as a peroxidase mimetic were also determined (Figure S17). The values of K_m and V_{max} for Ce-BPyDC, HRP, and other peroxidase mimics are listed in Table S2. Ce-BPyDC exhibited K_m values lower than that of HRP and other peroxidase mimics, suggesting that Ce-BPyDC has a higher affinity for both TMB and H_2O_2 . All of our results prove that Ce-BPyDC was an excellent artificial enzyme with dual enzyme-like activities.

Colorimetric Detection for Ascorbic Acid. Ascorbic acid (AA) is usually added to food sources as an artificial antioxidant in the food industry. AA is an indispensable type of vitamin for the good health of humans.⁴⁰ For instance, large doses of AA function as a pro-oxidant anticancer agent and can kill colorectal cancer cells selectively. Thus, precise detection of AA is of great significance in the fields of human health, food safety, and medical diagnosis.^{41–43} The blue oxTMB could be reduced to the colorless TMB with the participation of AA. Therefore, a colorimetric method for detecting AA was established with the advantages of simple operation and rapid, sensitive, and accurate detection. Under the optimized experimental conditions, a range of concentrations of the AA solution were added to the Ce-BPyDC/TMB system and the mixture was incubated for 10 min at room temperature. As one can see in Figure 4a, the more ascorbic acid is added (0–30

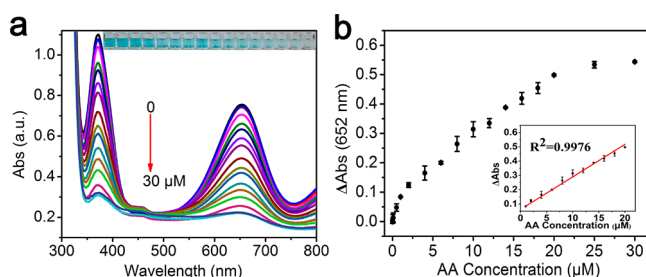


Figure 4. AA detection assay using Ce-BPyDC as an oxidase mimetic. (a) AA concentration-dependent ultraviolet–visible (UV–vis) absorption change. The inset photograph shows the visually recognizable color changes of the reaction system. (b) AA assay curve obtained from UV–vis spectral measurements. The inset shows the calibration curve. Conditions: $25 \mu\text{g mL}^{-1}$ Ce-BPyDC and 1 mM TMB, incubation in acetate buffer (pH 4.0) at room temperature for 10 min.

μM), the lower the absorption peak at 652 nm. The inset in Figure 4a shows the AA-dependent color changes of the test solutions, which could be discerned directly by the naked eye. The absorbance change at 652 nm as a function of the concentrations of AA changes is displayed in Figure 4b, and the inset shows a good linear correlation ($R^2 = 0.9976$) from 1 to 20 μM . On the basis of the 3S/N formula, the detection limit of this colorimetric method for AA detection could reach 0.28 μM . Compared with other colorimetric methods for AA determination (Table S3), our work has a lower detection limit, which indicated that this detection system was highly sensitive.

To explore the selectivity of our colorimetric probe for AA detection, some potential interfering substances, including K^+ , Na^+ , Ni^{2+} , Mn^{2+} , Cu^{2+} , Mg^{2+} , Ca^{2+} , Fe^{2+} , citric acid (CA), starch, fructose, sucrose, tartaric acid (TA), alanine (Ala), glycine (Gly), glutamate (Glu), and aspartic acid (Asp), were tested. The results (Figure 5) show that the interfering

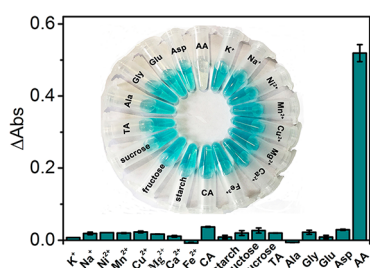


Figure 5. Selectivity test of AA over other coexisting substances in fruit juice. Condition: 20 μM AA, 2 mM other interfering substances.

substances have no apparent influence on absorbance even if the concentration was 100 times that of AA, indicating that the method exhibited excellent selectivity for AA. To further illustrate the real application of this method, this assay was used to analyze real samples (orange juice and grapefruit juice). As shown in Table 1, the detection results of the Ce-

Table 1. Detection of AA Contents in Fruit Juice Samples

sample	added (μM)	measured (μM)	AA test kit (μM)	recovery (%)	RSD (%) ($n = 3$)
orange juice	10	9.81	9.84	98.1	1.264
	20	20.33	19.68	101.7	2.236
grape juice	10	10.14	10.26	101.4	0.925
	20	19.24	20.12	96.2	1.749

BPyDC probe corresponded well with those of the commercial ascorbic acid kit (MAK074, Sigma). Moreover, using our method, the obtained recovery values of AA in fruit juice samples were between 96.2% and 101.7%. These results illustrate that this colorimetric detection of AA could be applied for practical AA detection in real samples. In summary, those results provide a strong basis for the potential application of Ce-BPyDC in the fields of biosensing, food analysis, and analytical chemistry.

CONCLUSION

In summary, we successfully synthesized a Ce-BPyDC by a facile method and found this material has dual enzyme activities (oxidase-like and peroxidase-like activities) in the

TMB oxidation reaction. It can be a readily available substitute for HRP and many similar nanozymes owing to its superior catalytic performance. The dual activities originated from the Ce(III)/Ce(IV) redox cycle system inside. On the basis of the oxidase-like catalytic activity, a colorimetric method for detecting AA was established with the advantages of simple operation and rapid, sensitive, and accurate detection, which could reach a linear range from 1 to 20 μM with a LOD of 0.28 μM . The detection of AA can be easily achieved by visible color fading without any instrumentation. Our work revealed the enzyme-like Ce-MOFs exhibited potential in food analysis and biosensing.

ASSOCIATED CONTENT

Supporting Information

The Supporting Information is available free of charge on the ACS Publications website at DOI: 10.1021/acs.inorgchem.9b00661.

Materials and methods, characterization (TEM, XPS, thermogravimetric analysis, and N_2 sorption isotherm), absorbance curves, optimization of conditions, optical photograph, stability tests, cycle experiments, scheme of the reaction mechanism, PL spectra, enzymatic kinetics, comparison of enzymatic activities, and comparison of methods (PDF)

AUTHOR INFORMATION

Corresponding Author

*E-mail: wanglong79@nwsuaf.edu.cn. Fax: +86 29-8709-2275. Telephone: +86 29-8709-2275.

ORCID

Jianlong Wang: 0000-0002-2879-9489

Notes

The authors declare no competing financial interest.

ACKNOWLEDGMENTS

The authors appreciate the kind support from the National Natural Science Foundation of China (21675127), the Shaanxi Provincial Science Fund for Distinguished Young Scholars (2018JC-011), the Development Project of Qinghai Provincial Key Laboratory (2017-ZJ-Y10), and the Capacity Building Project of Engineering Research Center of Qinghai Province (2017-GX-G03).

REFERENCES

- (1) Berglund, G. I.; Carlsson, G. H.; Smith, A. T.; Szöke, H.; Henriksen, A.; Hajdu, J. The catalytic pathway of horseradish peroxidase at high resolution. *Nature* **2002**, *417*, 463–468.
- (2) Wu, J.; Wang, X.; Wang, Q.; Lou, Z.; Li, S.; Zhu, Y.; Qin, L.; Wei, H. Nanomaterials with enzyme-like characteristics (nanozymes): next-generation artificial enzymes (II). *Chem. Soc. Rev.* **2019**, *48*, 1004–1076.
- (3) Jv, Y.; Li, B.; Cao, R. Positively-charged gold nanoparticles as peroxidase mimic and their application in hydrogen peroxide and glucose detection. *Chem. Commun.* **2010**, *46*, 8017–8019.
- (4) Gao, L.; Zhuang, J.; Nie, L.; Zhang, J.; Zhang, Y.; Gu, N.; Wang, T.; Feng, J.; Yang, D.; Perrett, S.; Yan, X. Intrinsic peroxidase-like activity of ferromagnetic nanoparticles. *Nat. Nanotechnol.* **2007**, *2*, 577–583.
- (5) Asati, A.; Santra, S.; Kaittanis, C.; Nath, S.; Perez, J. M. Oxidase-like activity of polymer-coated cerium oxide nanoparticles. *Angew. Chem.* **2009**, *121*, 2344–2348.

- (6) Feng, Y.-B.; Hong, L.; Liu, A.-L.; Chen, W.-D.; Li, G.-W.; Chen, W.; Xia, X.-H. High-efficiency catalytic degradation of phenol based on the peroxidase-like activity of cupric oxide nanoparticles. *Int. J. Environ. Sci. Technol.* **2015**, *12*, 653–660.
- (7) Purbia, R.; Paria, S. Green Synthesis of Single-Crystalline Akaganeite Nanorods for Peroxidase Mimic Colorimetric Sensing of Ultralow-Level Vitamin B1 and Sulfide Ions. *ACS Appl. Nano Mater.* **2018**, *1*, 1236–1246.
- (8) Huang, L.; Sun, D.-W.; Pu, H.; Wei, Q.; Luo, L.; Wang, J. A colorimetric paper sensor based on the domino reaction of acetylcholinesterase and degradable γ -MnOOH nanozyme for sensitive detection of organophosphorus pesticides. *Sens. Actuators, B* **2019**, *290*, 573–580.
- (9) Huang, L.; Chen, K.; Zhang, W.; Zhu, W.; Liu, X.; Wang, J.; Wang, R.; Hu, N.; Suo, Y.; Wang, J. ssDNA-tailorable oxidase-mimicking activity of spinel MnCo_2O_4 for sensitive biomolecular detection in food sample. *Sens. Actuators, B* **2018**, *269*, 79–87.
- (10) Zhu, W.; Zhang, J.; Jiang, Z.; Wang, W.; Liu, X. High-quality carbon dots: synthesis, peroxidase-like activity and their application in the detection of H_2O_2 , Ag^+ and Fe^{3+} . *RSC Adv.* **2014**, *4*, 17387–17392.
- (11) Huang, L.; Zhu, W.; Zhang, W.; Chen, K.; Wang, J.; Wang, R.; Yang, Q.; Hu, N.; Suo, Y.; Wang, J. Layered vanadium (IV) disulfide nanosheets as a peroxidase-like nanozyme for colorimetric detection of glucose. *Microchim. Acta* **2018**, *185*, 7.
- (12) Huang, L.; Zhu, Q.; Zhu, J.; Luo, L.; Pu, S.; Zhang, W.; Zhu, W.; Sun, J.; Wang, J. Portable Colorimetric Detection of Mercury(II) Based on a Non-Noble Metal Nanozyme with Tunable Activity. *Inorg. Chem.* **2019**, *58*, 1638–1646.
- (13) Wei, H.; Wang, E. Nanomaterials with enzyme-like characteristics (nanozymes): next-generation artificial enzymes. *Chem. Soc. Rev.* **2013**, *42*, 6060–6093.
- (14) Nasir, M.; Nawaz, M. H.; Latif, U.; Yaqub, M.; Hayat, A.; Rahim, A. An overview on enzyme-mimicking nanomaterials for use in electrochemical and optical assays. *Microchim. Acta* **2017**, *184*, 323–342.
- (15) Zhou, H.-C. J.; Kitagawa, S. Metal-organic frameworks (MOFs). *Chem. Soc. Rev.* **2014**, *43*, 5415–5418.
- (16) Zhang, W.; Shi, S.; Zhu, W.; Huang, L.; Yang, C.; Li, S.; Liu, X.; Wang, R.; Hu, N.; Suo, Y.; Li, Z.; Wang, J. Agar Aerogel Containing Small-Sized Zeolitic Imidazolate Framework Loaded Carbon Nitride: A Solar-Triggered Regenerable Decontaminant for Convenient and Enhanced Water Purification. *ACS Sustainable Chem. Eng.* **2017**, *5*, 9347–9354.
- (17) Zhang, L.; Wang, J.; Ren, X.; Zhang, W.; Zhang, T.; Liu, X.; Du, T.; Li, T.; Wang, J. Internally extended growth of core-shell NH_2 -MIL-101 (Al)@ ZIF-8 nanoflowers for the simultaneous detection and removal of Cu (ii). *J. Mater. Chem. A* **2018**, *6*, 21029–21038.
- (18) Kang, Z.; Fan, L.; Sun, D. Recent advances and challenges of metal-organic framework membranes for gas separation. *J. Mater. Chem. A* **2017**, *5*, 10073–10091.
- (19) Zhou, J.; Tian, G.; Zeng, L.; Song, X.; Bian, X. w. Nanoscaled Metal-Organic Frameworks for Biosensing, Imaging, and Cancer Therapy. *Adv. Healthcare Mater.* **2018**, *7*, 1800022.
- (20) Li, S.; Liu, X.; Chai, H.; Huang, Y. Recent advances in the construction and analytical applications of metal-organic frameworks-based nanozymes. *TrAC, Trends Anal. Chem.* **2018**, *105*, 391–403.
- (21) Ai, L.; Li, L.; Zhang, C.; Fu, J.; Jiang, J. MIL-53 (Fe): A Metal-Organic Framework with Intrinsic Peroxidase-Like Catalytic Activity for Colorimetric Biosensing. *Chem. - Eur. J.* **2013**, *19*, 15105–15108.
- (22) Liu, F.; He, J.; Zeng, M.; Hao, J.; Guo, Q.; Song, Y.; Wang, L. Cu-hemin metal-organic frameworks with peroxidase-like activity as peroxidase mimics for colorimetric sensing of glucose. *J. Nanopart. Res.* **2016**, *18*, 106.
- (23) Hu, Z.; Jiang, X.; Xu, F.; Jia, J.; Long, Z.; Hou, X. Colorimetric sensing of bithiols using photocatalytic UiO-66 (NH_2) as H_2O_2 -free peroxidase mimics. *Talanta* **2016**, *158*, 276–282.
- (24) Yin, Y.; Gao, C.; Xiao, Q.; Lin, G.; Lin, Z.; Cai, Z.; Yang, H. Protein-metal organic framework hybrid composites with intrinsic peroxidase-like activity as a colorimetric biosensing platform. *ACS Appl. Mater. Interfaces* **2016**, *8*, 29052–29061.
- (25) Yang, H.; Yang, R.; Zhang, P.; Qin, Y.; Chen, T.; Ye, F. A bimetallic (Co/2Fe) metal-organic framework with oxidase and peroxidase mimicking activity for colorimetric detection of hydrogen peroxide. *Microchim. Acta* **2017**, *184*, 4629–4635.
- (26) Chen, J.; Shu, Y.; Li, H.; Xu, Q.; Hu, X. Nickel metal-organic framework 2D nanosheets with enhanced peroxidase nanozyme activity for colorimetric detection of H_2O_2 . *Talanta* **2018**, *189*, 254–261.
- (27) Qin, F.-X.; Jia, S.-Y.; Wang, F.-F.; Wu, S.-H.; Song, J.; Liu, Y. Hemin@ metal-organic framework with peroxidase-like activity and its application to glucose detection. *Catal. Sci. Technol.* **2013**, *3*, 2761–2768.
- (28) Qin, L.; Wang, X.; Liu, Y.; Wei, H. 2D-Metal-Organic-Framework-Nanozyme Sensor Arrays for Probing Phosphates and Their Enzymatic Hydrolysis. *Anal. Chem.* **2018**, *90*, 9983–9989.
- (29) Haque, N.; Hughes, A.; Lim, S.; Vernon, C. Rare earth elements: Overview of mining, mineralogy, uses, sustainability and environmental impact. *Resources* **2014**, *3*, 614–635.
- (30) Zhang, F.; Wang, P.; Koberstein, J.; Khalid, S.; Chan, S.-W. Cerium oxidation state in ceria nanoparticles studied with X-ray photoelectron spectroscopy and absorption near edge spectroscopy. *Surf. Sci.* **2004**, *563*, 74–82.
- (31) Montini, T.; Melchionna, M.; Monai, M.; Fornasiero, P. Fundamentals and catalytic applications of CeO_2 -based materials. *Chem. Rev.* **2016**, *116*, 5987–6041.
- (32) Huang, L.; Zhang, W.; Chen, K.; Zhu, W.; Liu, X.; Wang, R.; Zhang, X.; Hu, N.; Suo, Y.; Wang, J. Facet-selective response of trigger molecule to CeO_2 {110} for up-regulating oxidase-like activity. *Chem. Eng. J.* **2017**, *330*, 746–752.
- (33) Xiong, Y.; Chen, S.; Ye, F.; Su, L.; Zhang, C.; Shen, S.; Zhao, S. Synthesis of a mixed valence state Ce-MOF as an oxidase mimetic for the colorimetric detection of biothiols. *Chem. Commun.* **2015**, *51*, 4635–4638.
- (34) Dalapati, R.; Sakthivel, B.; Ghosal, M. K.; Dhakshinamoorthy, A.; Biswas, S. A cerium-based metal-organic framework having inherent oxidase-like activity applicable for colorimetric sensing of biothiols and aerobic oxidation of thiols. *CrystEngComm* **2017**, *19*, 5915–5925.
- (35) Lammert, M.; Glißmann, C.; Reinsch, H.; Stock, N. Synthesis and characterization of new Ce (IV)-MOFs exhibiting various framework topologies. *Cryst. Growth Des.* **2017**, *17*, 1125–1131.
- (36) Yu, H.; Han, J.; An, S.; Xie, G.; Chen, S. Ce (III, IV)-MOF electrocatalyst as signal-amplifying tag for sensitive electrochemical aptasensing. *Biosens. Bioelectron.* **2018**, *109*, 63–69.
- (37) Tao, Y.; Ju, E.; Ren, J.; Qu, X. Bifunctionalized mesoporous silica-supported gold nanoparticles: intrinsic oxidase and peroxidase catalytic activities for antibacterial applications. *Adv. Mater.* **2015**, *27*, 1097–1104.
- (38) Ge, S.; Liu, F.; Liu, W.; Yan, M.; Song, X.; Yu, J. Colorimetric assay of K-562 cells based on folic acid-conjugated porous bimetallic Pd@Au nanoparticles for point-of-care testing. *Chem. Commun. (Cambridge, U. K.)* **2014**, *50*, 475–477.
- (39) Buxton, G. V.; Greenstock, C. L.; Helman, W. P.; Ross, A. B. Critical review of rate constants for reactions of hydrated electrons, hydrogen atoms and hydroxyl radicals ($\bullet\text{OH}/\text{O}^-$) in aqueous solution. *J. Phys. Chem. Ref. Data* **1988**, *17*, 513–886.
- (40) Wu, D.; Li, Y.; Zhang, Y.; Wang, P.; Wei, Q.; Du, B. Sensitive Electrochemical Sensor for Simultaneous Determination of Dopamine, Ascorbic Acid, and Uric Acid Enhanced by Amino-group Functionalized Mesoporous Fe_3O_4 @Graphene Sheets. *Electrochim. Acta* **2014**, *116*, 244–249.
- (41) Cheng, H.; Wang, X.; Wei, H. Ratiometric electrochemical sensor for effective and reliable detection of ascorbic acid in living brains. *Anal. Chem.* **2015**, *87*, 8889–8895.
- (42) Huang, L.; Sun, D.; Pu, H.; Wei, Q. Development of Nanozymes for Food Quality and Safety Detection: Principles and

Recent Applications. *Compr. Rev. Food Sci. Food Saf.* **2019**, DOI: 10.1111/1541-4337.12485.

(43) Qin-Jiang, Z.; Jin, W.; Qiu-E, C.; Chuan-Hua, Z. Construction and Application of Target-induced Silver Deposition Based Colorimetric Assay. *Fenxi Huaxue* **2018**, *46*, 1215–1221.